AGU PUBLICATIONS

JGR

Journal of Geophysical Research: Space Physics

REGULAR ARTICLE

10.1002/2013JA018964

Key Points:
- Vortical flow associated to FTEs
- Single FTE signatures
- Three-dimensional non-antiparallel magnetic fields

Correspondence to:
J. C. Santos,
jeansantos@unb.br

Citation:
Santos, J. C., D. G. Sibeck, J. Büchner, W. D. Gonzalez, and J. L. Ferreira (2014), Three-dimensional MHD simulation of FTEs produced by merging at an isolated point in a sheared magnetic field configuration, *J. Geophys. Res. Space Physics*, *119*, 2009–2023, doi:10.1002/2013JA018964.

Received 19 APR 2013
Accepted 4 DEC 2013
Accepted article online 10 DEC 2013
Published online 27 MAR 2014

Three-dimensional MHD simulation of FTEs produced by merging at an isolated point in a sheared magnetic field configuration

J. C. Santos[1,2], D. G. Sibeck[3], J. Büchner[4], W. D. Gonzalez[5], and J. L. Ferreira[1]

[1]Instituto de Física, Universidade de Brasília, Brasília, Brazil. [2]Departamento de Física, Universidade Tecnológica Federal do Paraná, Curitiba, Brazil. [3]NASA/GSFC, Greenbelt, Maryland, USA. [4]Max Planck Institut für Sonnensystemforschung, Katlenburg-Lindau, Germany. [5]Instituto Nacional de Pesquisas Espaciais, São José dos Campos, Brazil.

Abstract We present predictions for the evolution of FTEs generated by localized bursts of reconnection on a planar magnetopause that separates a magnetosheath region of high densities and weak magnetic field from a magnetospheric region of low densities and strong magnetic field. The magnetic fields present a shear angle of 105 degrees. Reconnection forms a pair of FTEs each crossing the magnetopause in the field reversal region and bulging into the magnetosphere and magnetosheath. At their initial stage they can be characterized as flux tubes since the newly reconnected magnetic field lines are not twisted. Reconnection launches Alfvenic perturbations that propagate along the FTEs generating high-speed jets, which move the pair of FTEs in opposite directions. As the FTE moves, it displaces the ambient magnetic field and plasma producing bipolar magnetic field and plasma velocity signatures normal to the nominal magnetopause in the regions surrounding the FTE. The combination of the ambient plasma with the FTE flows generates a vortical velocity pattern around the reconnected field lines. During its evolution the FTE evolves to a flux rope configuration due to the twist of the magnetic field lines. The alfvenic perturbations propagate faster along the part of the FTE bulging into the magnetosphere than in the magnetosheath, and due to the differences between the plasma and magnetic field properties the perturbations have slightly different signatures in the two regions. As a consequence, the FTEs have different signatures depending on whether the satellite encounters the part bulging into the magnetosphere or into the magnetosheath.

1. Introduction

Flux transfer events (FTEs) have been interpreted as the result of transient and localized reconnection occurring at the dayside magnetopause [*Russell and Elphic*, 1978]. They occur frequently [*Rijnbeek et al.*, 1984] and are believed to be responsible for a significant fraction of the flux transport from the dayside to nightside magnetosphere [*Cowley*, 1984]. In satellite data, they are characterized by a positive-negative (standard FTE) or a negative-positive (reverse FTE) pulse in the component of the magnetic field perpendicular to the nominal magnetopause (B_N). This pulse is thought to result from the draping of the ambient magnetic field lines around the reconnected flux tube combined with the formation of an axial field-aligned current along the flux tube itself [*Paschmann et al.*, 1982]. The field-aligned current along the FTE is associated with a twist in the field and allows the interpretation of FTEs as a flux rope instead of a flux tube [*Paschmann et al.*, 1982]. The total field magnitude inside the FTE can be characterized by an overall peak or a decrease (crater), the latter being suggested as an initial stage of FTE evolution [*Zhang et al.*, 2010]. The decrease in the total field in crater FTEs consists of two "trenches" in the magnetic field at the edges of the crater, with a slight increase in the field in the center reflecting the existence of a weak force-free helical current similar to that observed in flux ropes [*LaBelle et al.*, 1987]. Support for the hypothesis that FTEs are flux ropes instead of flux tubes is also given in *Zhang et al.* [2008] where magnetic field observations from multiple satellites were fitted to a flux rope model. Other features appearing to be invariant characteristics of FTE are a mixture of magnetospheric and magnetosheath particle populations and an increase in the total pressure inside the FTE compared to that outside the event [*Paschmann et al.*, 1982].

Once FTEs form, they move across the magnetopause plane, away from the reconnection site, in response to pressure gradient and curvature forces [*Cooling et al.*, 2001]. *Dailey et al.* [1985] investigated a series of 23 FTE events and determined an average $\vec{E} \times \vec{B}$ drift velocity of 125 km/s for the reconnected flux tube.

In investigating the spatial properties of FTEs using ISEE 1 and 2 satellite data, *Saunders et al.* [1984] reported the first evidence for plasma vorticity in or around FTEs tubes. They associated this vorticity with magnetic field twisting and a torsional Alfvén wave propagating antiparallel to the ambient field. *Liu et al.* [2008] found, using Time History of Events and Macroscale Interactions during Substorms (THEMIS) multiple satellite data, that flow perturbations outside of FTEs in the magnetosphere are approximately dipolar.

Korotova et al. [2009] developed a flow signature taxonomy for FTEs. For events moving faster than the ambient media the flow perturbation directly upstream and downstream from the events should be in the direction of the event motion. Flows on the flanks should be opposite to event motion. They should also be accompanied by bipolar inward/outward (outward/inward) flow perturbations normal to the nominal magnetopause in the magnetosphere (magnetosheath). Events moving with the ambient flow should generate no flow perturbations in the ambient plasma. Alfvén waves propagating parallel (antiparallel) to the FTE's axial magnetic field should generate anticorrelated (correlated) flow perturbations within the core region of FTEs.

Farrugia et al. [1987] developed a simple incompressible flow model for the interaction of the ambient field and fluid with a rigid flux tube of cylindrical geometry. The flow obtained was a classical potential flow ($\vec{\nabla} \times \vec{v} = 0$), and with a knowledge of the flow field from hydrodynamics, the magnetic field could also be determined. Their results show that plasma approaching the tube is decelerated and deflected at the periphery of the tube. The flow has a dipolar form in the rest frame of the flux tube, and the magnetic field perturbations obtained from this flow resemble FTE signatures. The normal component executes a bipolar excursion about zero, while the tangential components suffer substantial changes which maximize when B_N passes through zero.

Recently, *Zhang et al.* [2011] investigated the flow properties around 3701 FTEs observed between May and October in both 2007 and 2008 by THEMIS spacecraft. The flow perturbations observed in conjunction with the magnetic signatures show that FTEs moving in an antisunward direction on the magnetopause are associated with flow vortices just inside the magnetopause. In order to understand the flow perturbations they have developed a 2-D MHD model that starts from the solution obtained by *Farrugia et al.* [1987] but remove the assumption that the flow is inviscid and impose finite viscosity near the FTE. They conclude that viscosity plays a key role in the formation of flow vortices in the low-latitude boundary layer, and when it is considered the simulation reproduces the observations qualitatively. However, they do not discuss the mechanism responsible for the increase in viscosity close to the FTE nor investigate the evolution of magnetic field and plasma inside the FTE.

Ku and Sibeck [1997, 1998a, 1998b, 2000] performed a series of 2-D magnetohydrodynamic (MHD) simulations to investigate the signatures of FTEs produced by a Petschek-type reconnection occurring close to the subsolar point. In their first work [*Ku and Sibeck*, 1997] reconnection is started by a step function time-dependent localized increase in resistivity. The plasma is at rest at the beginning of the simulation, and the initial magnetosheath and magnetosphere field and plasma parameters are chosen in a way to reproduce realistic ratios observed by satellites for the magnetosheath-magnetosphere system. They observe that a bulge of merged field lines develops almost entirely on the magnetosheath side of the magnetopause and grows with time. The bulge moves along the magnetopause at a fraction of the magnetosheath Alfvén speed. A plasma jet in the direction of the bulge's motion forms in a boundary layer on the magnetospheric side of the magnetopause. This jet is on magnetic field lines with depressed magnetic field strengths and approach and slightly exceeds the magnetosheath Alfvén velocities. Outside the bulge a gentler reverse flow appears on the magnetosheath side. This reverse flow is associated with a vortical structure that follows the bulge during its motion. *Ku and Sibeck* [1998a] found that events moving opposite to a background magnetosheath flow slow down but intensify, whereas events moving in the direction of the magnetosheath flow accelerate but weaken. The vortical flow outside the bulge on the magnetosheath is weakened for events moving in the direction of the magnetosheath flow, whereas it is strengthened for events moving opposite to the flow. They associate the FTEs signature with the vortical flow at the magnetosheath. *Ku and Sibeck* [1998b] checked for the effects of bursty reconnection and secondary reconnection by considering a background resistivity and turning on and off the enhanced local resistivity. In this case after the enhanced resistivity is switched off, secondary reconnection sites appear on the trailing edge of the event where thin current sheets are formed. Merging at these sites inflates and propels the main FTE. They also fill a magnetic island with hot tenuous plasma near the subsolar point. Transient magnetic islands

also form on the trailing edge of the main FTE, forming secondary FTEs, but they remain small and later disappear. Besides giving important information about FTE evolution and the associated perturbation in the ambient plasma and magnetic field, the 2-D simulations performed in *Ku and Sibeck* [1997, 1998a, 1998b, 2000] only consider perfectly antiparallel fields, a particular case that is rarely observed at the magnetopause. Also, in their 2-D simulations the FTE evolution is restricted to the plane perpendicular to the magnetopause as well as the evolution of associated perturbations. The combination of these two facts leads to the interpretation of the FTE as the bulge forming close to the field reversal region and caused difficulties in separating magnetospheric from magnetosheath evolution.

Global simulations to investigate the generation mechanisms of FTEs have been performed by *Fedder et al.* [2002], *Raeder* [2006], and *Dorelli and Bhattacharjee* [2009]. *Fedder et al.* [2002] reported that the FTE is formed via global separator reconnection. They invoke a current-driven instability as the driver of reconnection, and as separator reconnection proceeds, strong parallel currents form along the reconnected flux tube, resulting in a twist of the field lines. *Raeder* [2006] had investigated the generation mechanism of FTEs during strongly southward interplanetary magnetic field. In his simulations FTEs are generated by multiple X line reconnection. The multiple X lines form sequentially for periods of significant dipole tilt. This gives a seasonally modulated formation rate for FTEs, with no FTE formation during equinox and formation in the winter hemisphere during solstices. The model explains the 8 min quasiperiodicity by the convection and reformation time of flux ropes at the magnetopause. In the *Dorelli and Bhattacharjee* [2009] simulation as the subsolar magnetopause current density grows in time, the local geometry of the magnetic field changes in such a way that the stagnation point of the flow moves away from the subsolar point, producing a large flow shear at the subsolar magnetopause. The subsolar flow shear is unstable to the formation of flow vortices, which grow and coalesce as the FTE grows at the subsolar magnetopause. The flow vortices within the FTE drive 3-D magnetic reconnection resulting in a complex magnetic topology. In performing global simulations, the authors focused mainly on the generation mechanisms of FTEs and not on the 3-D evolution of reconnected magnetic field lines and associated plasma and magnetic field perturbation. Also, as stressed by *Dorelli and Bhattacharjee* [2009], reconnection in the case of *Fedder et al.* [2002] and *Raeder* [2006] are due numerical resistivity, and the results obtained in the simulation by *Raeder* [2006] and *Dorelli and Bhattacharjee* [2009] for plasma temperature and density inside the FTEs are not in agreement with observations.

In this work we extended the investigations performed in *Ku and Sibeck* [1997, 1998a, 1998b, 2000] by using a local 3-D resistive MHD simulations and considering a sheared magnetic field configuration. Similar work has been performed by *Otto* [1990, 1995], *Ma et al.* [1995], *La Belle-Hamer et al.* [1995], and *Otto et al.* [1995]. Here we focus on the 3-D nature of the flow in and around the FTE during its evolution and the differences in the FTE signature and related perturbation in the magnetosheath and magnetosphere plasma and magnetic field. In section 2 we present the model equations, initial, and boundary conditions. In section 3 we present the results obtained in our numerical experiment. Finally, in section 4, we summarize our findings and draw our conclusions.

2. Model Setup

The model used to perform this work was successfully applied to study the evolution of plasma and magnetic field in the solar atmosphere [*Santos and Büchner*, 2007; *Santos et al.*, 2008, 2011a, 2011b]. It solves an appropriate set of resistive MHD equations (in normalized units)

$$\frac{\partial \rho}{\partial t} = -\vec{\nabla} \cdot \rho\vec{u} \tag{1}$$

$$\frac{\partial \rho\vec{u}}{\partial t} = -\vec{\nabla} \cdot \rho\vec{u}\vec{u} - \vec{\nabla}p + \vec{j} \times \vec{B} \tag{2}$$

$$\frac{\partial \vec{B}}{\partial t} = \vec{\nabla} \times (\vec{u} \times \vec{B} - \frac{1}{\mu_0}\eta\vec{j}) \tag{3}$$

$$\frac{\partial p}{\partial t} = -\vec{\nabla} \cdot p\vec{u} - (\gamma - 1)p\vec{\nabla} \cdot \vec{u} + \frac{2(\gamma - 1)}{\beta_0}\eta j^2 \tag{4}$$

Table 1. Values Used for the Normalization of the Macroscopic Variables

Macroscopic Variable	Normalization Value
B	$B_0 = 1 \times 10^{-8}$ T
L	$L_0 = 4 \times 10^5$ m
T	$T_0 = 10^6$ K
p	$p_0 = \beta_0 \frac{B^2}{2\mu_0} = 3.6 \times 10^{-11}$ Pa
ρ	$\rho_0 = \frac{p_0 m_p}{2\kappa_B T_0} = 2.2 \times 10^{-21}$ kg
υ	$\upsilon_0 = \upsilon_A = \frac{B_0}{\sqrt{\mu_0 \rho_0}} = 191,642$ m/s
t	$t_0 = \frac{L_0}{\upsilon_0} = 2.1$ s

together with Ohm's law, Ampère's law, and taking into account the ideal gas equation for a fully ionized plasma

$$\vec{E} = -\vec{u} \times \vec{B} + \eta \vec{j} \tag{5}$$

$$\vec{\nabla} \times \vec{B} = \mu_0 \vec{j} \tag{6}$$

$$p = 2n\kappa_B T \tag{7}$$

Here ρ is the plasma mass density, $\vec{u}$ is the plasma velocity, $\vec{B}$ is the magnetic field, p is the plasma pressure, T is the plasma temperature, β_0 is the normalization value used for the plasma beta, and γ is the polytropic index ($\gamma = \frac{5}{3}$). Table 1 presents the values used in the normalization of the macroscopic variables.

The system of equations is solved in an equidistant cartesian grid ($131 \times 131 \times 131$ grid points) that covers a 3-D volume of $12 \times 24 \times 32$ Mm^3. This gives a grid resolution of approximately $91 \times 183 \times 244$ km in x, y and, z directions, respectively. The equations are solved using a second-order scheme in time (Leapfrog) and a second-order scheme in space (centered differences). The simulation volume presents six boundaries: four lateral, top, and bottom boundaries. We apply Neumann boundary conditions on all boundaries with $\frac{df}{dt} = 0$, apart on the lateral boundaries where we have considered the boundary closed for perpendicular flows. In this way we allow a free outflow on the top and bottom boundaries and a reflective flow on the other four boundaries. We keep $\vec{\nabla} \cdot \vec{B}$ close to zero by applying the projection method for divergence cleaning [*Tóth*, 2000].

The initial conditions for the plasma and magnetic field are the same used in *Otto* [1990] and represent a planar current sheet (the magnetopause) which separates regions of different plasma properties. These initial conditions are reproduced below:

$$\rho(x) = \rho_1 + \rho_2 \tanh\left(\frac{x - x_0}{d_x}\right) \tag{8}$$

$$p_x(x) = p_{00} + 2b_{z0}\Delta_b \tanh x + (1 - \beta_0)\Delta_b^2 \cosh^{-2} x \tag{9}$$

$$b_y(x) = \sqrt{b_{y0}^2 + \beta_0 \Delta_b^2 \cosh^{-2} x} \tag{10}$$

$$b_z(x) = b_{z0} - \Delta_b \tanh x \tag{11}$$

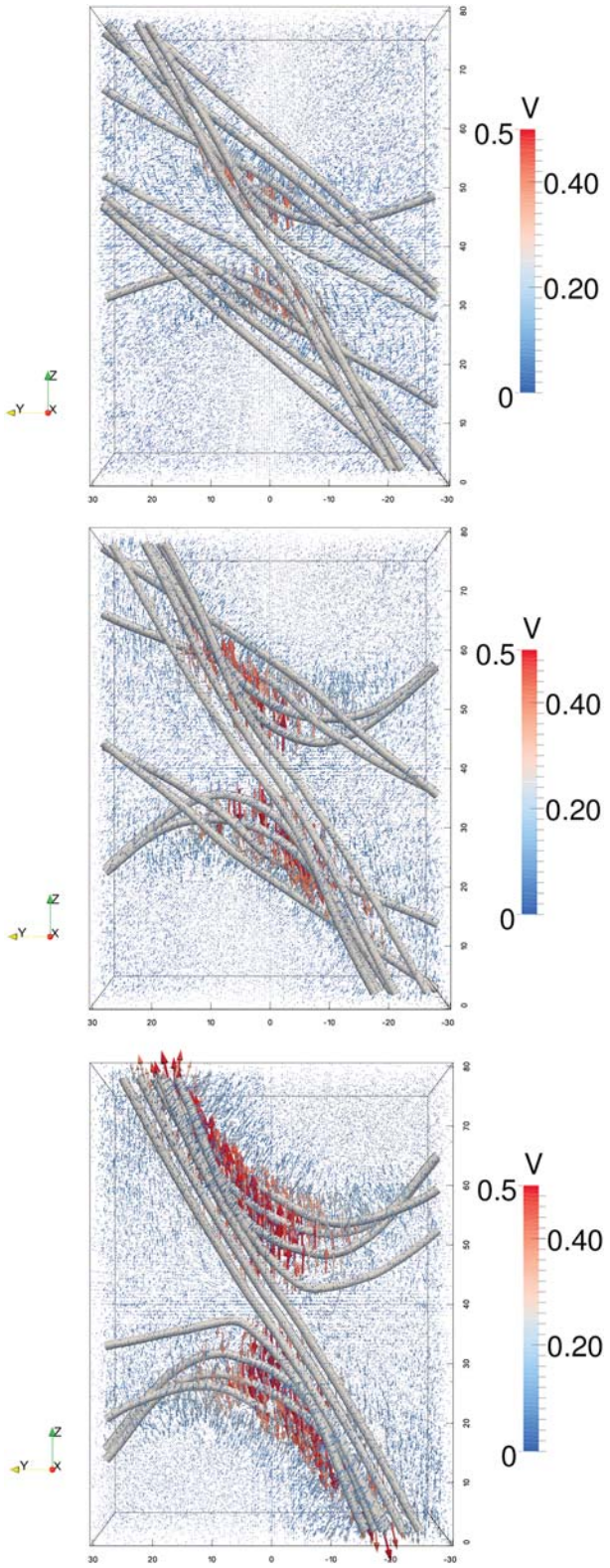

Figure 1. Time evolution of the magnetic field (tubes) and plasma flow (arrows) for simulation of FTE formation via localized Petschek reconnection. (top to bottom) The snapshots show results at $t = 210$ s, 294 s, and 378 s. The view is in the positive x direction and macroscopic variables are presented in normalized units.

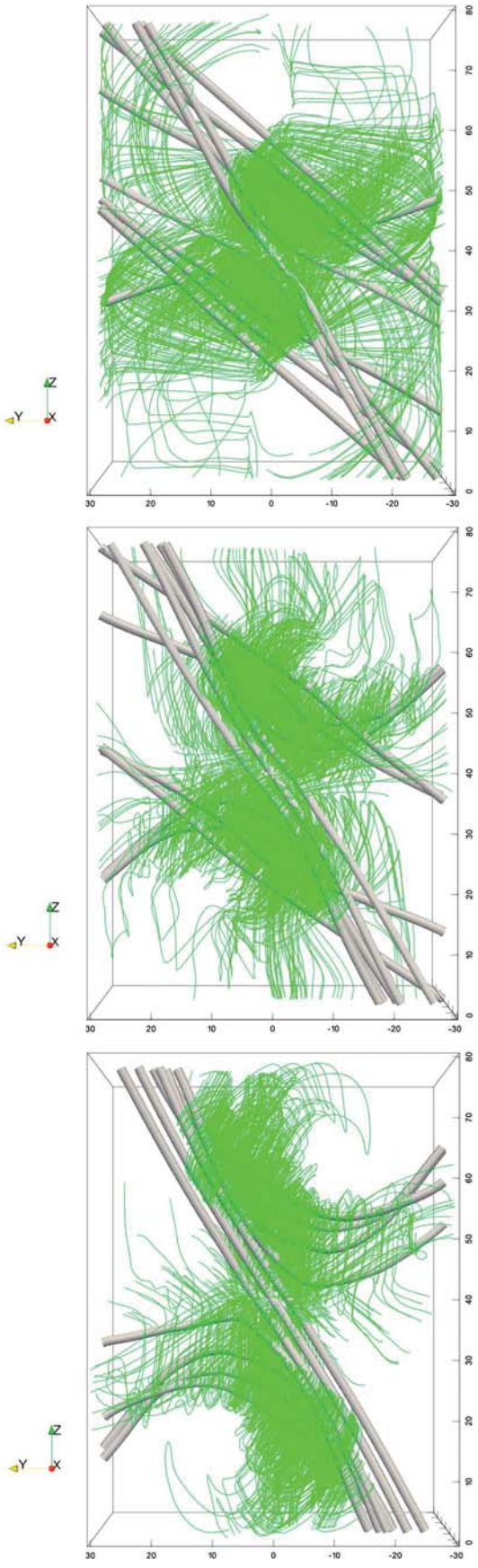

with

$$\Delta_b = 0.5\sqrt{1 + b_{sh}^2 - 2b_{sh}\cos\delta}$$

$$b_{z0} = \frac{1 - b_{sh}^2}{4\Delta_b}$$

$$b_{y0} = \frac{b_{sh}\sin\delta}{2\Delta_b}$$

The free parameters δ, b_{sh}, and p_{00} determine the asymptotic magnetic shear, the amplitude of the magnetic field in the magnetosheath (normalized units), and the typical thermal pressure (normalized units). The additional parameters ρ_1, ρ_2, x_0, and d_x determine the jump in mass density (normalized units), the position, and width of the transition region where the jump occurs. Magnetosheath plasma is initially at rest since we consider reconnection near the stagnation point. However, as stressed by *Korotova et al.* [2009], the flow results obtained in this situation can also be applied to the situation when the FTE moves faster than the ambient plasma. As in *Otto* [1990], the *y* and *z* directions do not correspond to the *y* and *z* directions described in GSE or GSM coordinate systems.

In Petschek's model [*Petschek*, 1964] dissipation occur within a small region inside the current sheet, known as the diffusion region. In the diffusion region, disruption of the current leads to the breakdown of the frozen-in approximation allowing reconnection to occur. In view of the fact that the physical process giving rise to reconnection, which is believed to be microscopic in nature, is still a matter of debate, we consider reconnection as initiated by a spot of localized increase in magnetic diffusivity [*Büchner and Elkina*, 2005, 2006]. As in *Otto* [1990] we assume that the localized magnetic diffusivity is present for $t \geq 0$ and is given by

$$\eta(x,y,z) = \eta_a \cosh^{-2}\frac{x}{3}\cosh^{-2}\frac{y}{3}\cosh^{-2}\frac{z-40}{3}. \quad (12)$$

where η_a is the anomalous magnetic diffusivity.

3. Simulation Results

We perform a numerical experiment to investigate the properties of FTEs formed by a

Figure 2. Time evolution of the magnetic field (tubes) and flow field lines for simulation of FTE formation via localized Petschek reconnection. (top to bottom) The snapshots show results at $t = 210$ s, 294 s, and 378 s. The view is in the positive *x* direction.

localized Petschek-type reconnection in a 3-D space and its influence in the ambient plasma and magnetic field in the course of its evolution. This mechanism for generating FTEs goes back to the mechanism suggested by *Russell and Elphic* [1978]. The merging occurs at a magnetopause marked by sharp transitions in density, temperature, and magnetic field strength and direction. The ratio of magnetosheath to magnetospheric densities is 4, the ratio of field strengths is 0.75, and that of temperatures is 0.385. The magnetic field is subject to a shearing of approximately 105° close to the plane defined by $x = 0$ (magnetopause). The magnetosheath region is located at $x > 0$, while the magnetosphere is located at $x < 0$.

The merging occurs due to a localized increase in the magnetic diffusivity (anomalous diffusivity, *Büchner and Elkina* [2005, 2006]) in a region around the center of the simulation box, known as diffusion region, where the normalized values of the diffusivity increase from zero to a peak value of 0.05 in normalized units. The increase in magnetic diffusivity causes a localized breakdown of the frozen-in approximation, allowing the field to change connectivity. This region also acts as a localized source of reconnection electric field and accompanying disturbances, as well as a generator of magnetohydrodynamic (MHD) waves. The MHD waves propagate rapidly outward from the dissipation region, along the reconnected field lines, and dominate energy conversion on large scale.

Figure 1 presents a 3-D visualization of plasma flow (arrows) and magnetic field (tubes) patterns at three different times following the onset of reconnection ($t = 210$ s, 294 s, and 378 s). The magnetic field lines start on points along a line going from $z = 20_0$ to $z = 60L_0$, at the plane $x = 0$. The length of the arrows are proportional to the magnitude of the flow velocities. The color code depicts the velocity magnitude saturated

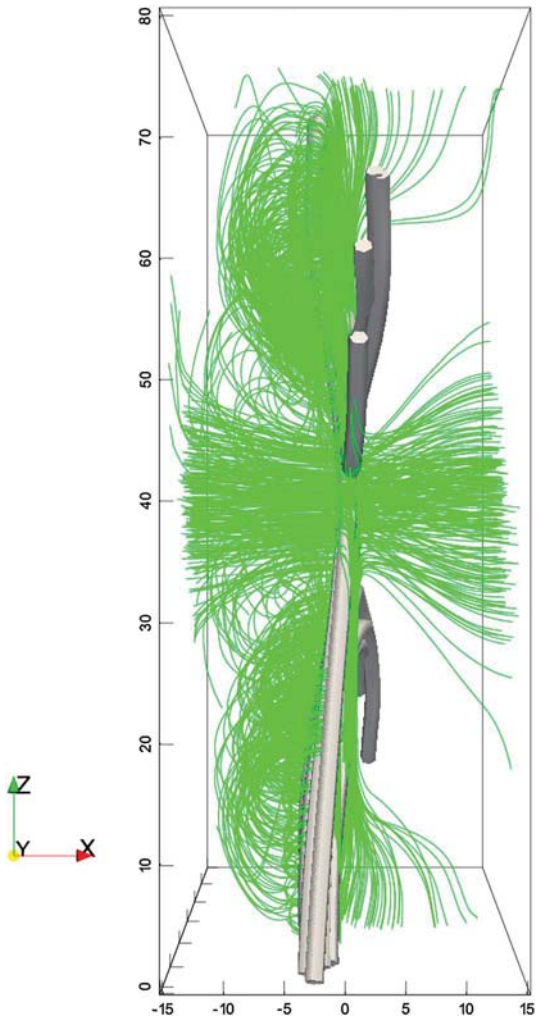

Figure 3. Lateral view of magnetic field (tubes) and flow field lines at $t = 378$ s. The view is in the positive y direction.

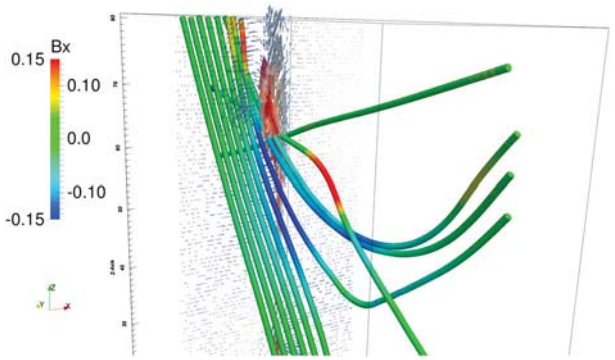

Figure 4. Vortical flow around FTE 1 at $t = 378$ s. The magnetic field (tubes) is colored with the x component of the field, in normalized units, while the velocity vectors (arrows) are colored by the velocity magnitude.

at $0.5v_0$, where v_0 is the normalization velocity (see Table 1), for better visualization. Reconnection takes place within a spherical region of radius $\approx 5L_0$, where L_0 is the normalization length scale (see Table 1), with center located at $(x_0, y_0, z_0) = (0, 0, 40)$ in normalized units. Two regions of merged field lines develop and move along the magnetopause, above, and below the diffusion region in the z direction. In the region above $z = 40$ plasma is accelerated mainly in the positive z direction, while in the region below $z = 40$ plasma is accelerated mainly in the negative z direction. These are the outflow jets characteristic of the reconnection process. Figure 1a shows that at $t = 210$ s plasma is accelerated only in regions close to the diffusion region. However, reconnection generates MHD waves which propagate rapidly outward from the dissipation region along the reconnected field lines. The velocity of propagation of these waves is larger in the magnetosphere than in the magnetosheath, because the Alfvén velocity is larger there. As a consequence, energy conversion is expected to take place faster along the part of the reconnected field lines that bulges into the magnetosphere than on the part that bulges into the magnetosheath. Figure 1c shows that at $t = 378$ s the plasma jets have been formed along the part of the reconnected magnetic field lines that bulges into the magnetosphere, reaching the top and bottom of the simulation box. The jets do not form much further away from the diffusion region along the part of the reconnected field lines that bulges into the magnetosheath. At $t = 378$ s the plasma velocity peaks at approximately $0.7v_0$, which corresponds to 134 km/s. This value is very close to the average value of 125 km/s found observationally by *Dailey et al.* [1985] for the average $\vec{E} \times \vec{B}$ drift velocity of the reconnected flux tubes. The maximum Alfvén mach number obtained in the simulation volume at this time is about 1.3 in a region close to the diffusion region.

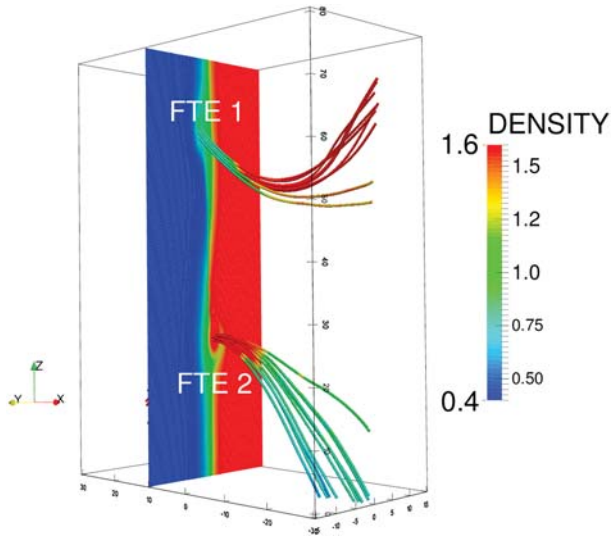

Figure 5. Magnetic field associated to the flux transfer event 1 (FTE 1) and flux transfer event 2 (FTE 2) at $t = 378$ s. Also shown is the density in a plane intersecting the two FTEs at $y = 10L_0$. The color code depicts the density variation in normalized units.

Associated with the plasma jets that form along the reconnected field lines, there is a vortical plasma flow. This vortical flow pattern is not visible in Figure 1 because it is very weak compared to the plasma jet generated in the process. Figure3 shows the magnetic field and flow field lines at $t = 210$ s, 294 s, and 378 s. It is visible from this figure that the flow field lines gradually concentrate around the part of the reconnected field lines that bulges into the magnetosphere. Figure 3 shows a lateral view of Figure 3c. The vortical plasma flow is on the magnetospheric side, and it closes on the plasma jet. The vortical flow also appears around the part of the reconnected field lines that bulges into the magnetosheath but does not form much further away from the diffusion region. Figure 4 shows the velocity vectors in a plane at $y = 10$. We draw field lines starting in a region on that plane close to the center of the vortex and along a line in the x direc-

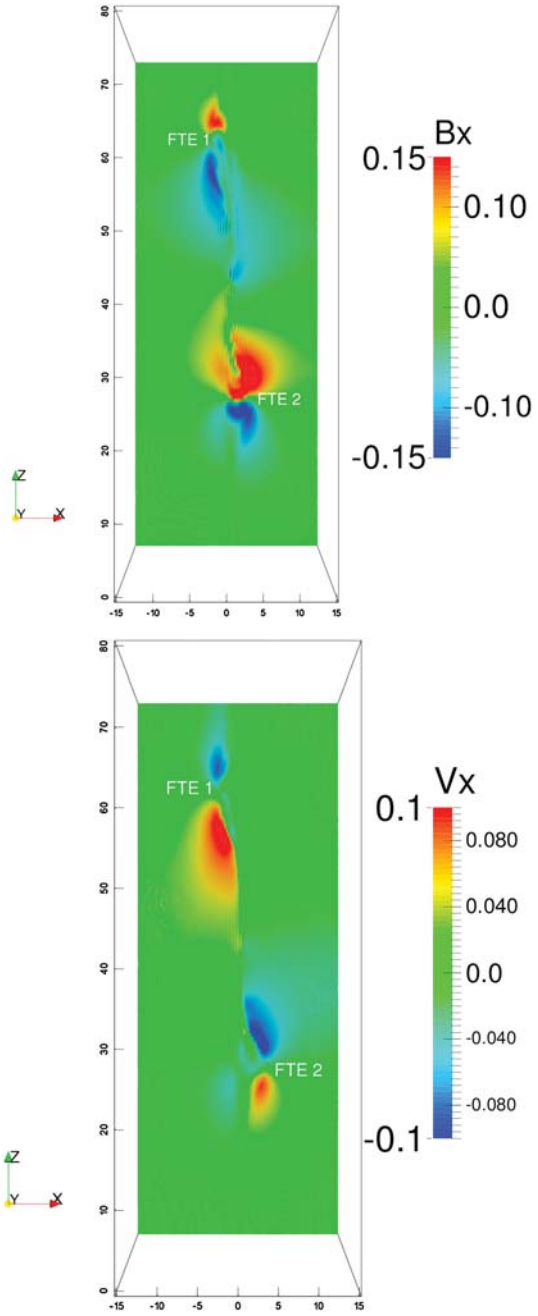

Figure 6. (top) Component of the magnetic field and (bottom) plasma velocity perpendicular to the nominal magnetopause at a xz plane located at $y = 10L_0$, for $t = 378$ s. The view is in the positive y direction, and macroscopic variables are presented in normalized units.

tion that crosses the vortex region in the plane $y = 10$. The field lines obtained are a combination of open (reconnected) and closed field lines. From the figure it seems that the strong jets are on closed field lines and the vortical structure is due the motion of the plasma around the reconnected field lines. This is similar to the situation described in *Korotova et al.* [2009] and in the model of *Farrugia et al.* [1987]. There is also a flow perpendicular to the diffusion region, along the *x* direction. This flow brings magnetic flux from the magnetosheath and magnetosphere to feed the reconnection process.

We now analyze the spatial variation of the plasma parameters associated to the FTE. Different from the 2-D simulations performed by *Ku and Sibeck* [1997, 1998a, 1998b, 2000] or in cases where the magnetosheath and magnetospheric magnetic fields are perfectly antiparallel, here the FTE signature is not anymore associated to the bulge that forms around the field reversal region but it is distributed along the reconnected field lines as the Alfvenic perturbation propagates from the reconnection point. As a consequence, we can follow the evolution of the part of the FTE bulging into the magnetosphere and the part bulging into the

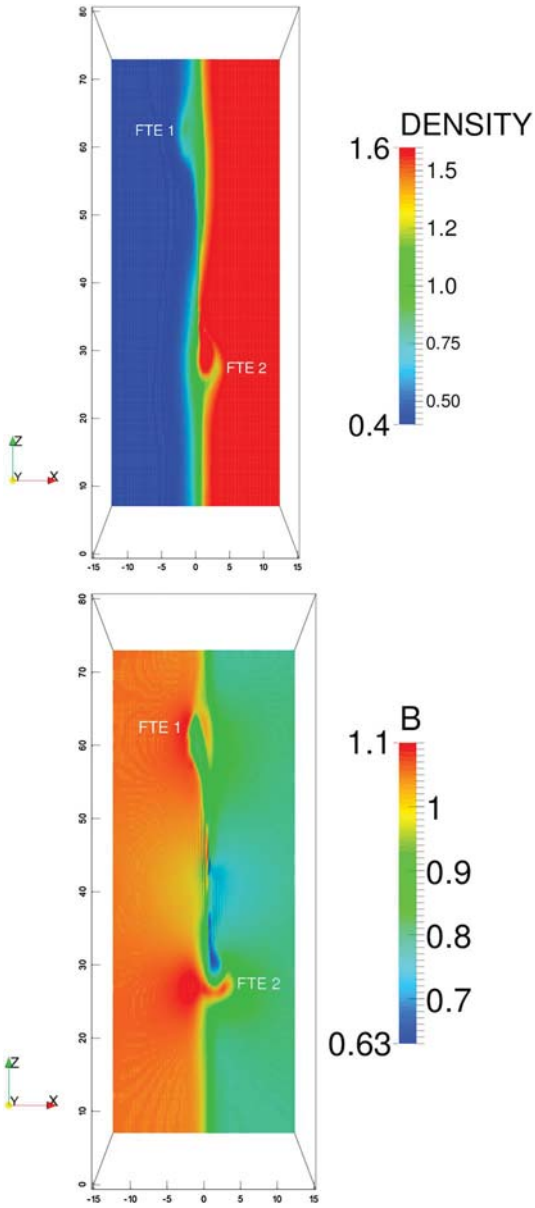

Figure 7. (top) Plasma density and (bottom) total magnetic field intensity at a *xz* plane located at $y = 10L_0$, for $t = 378$ s. The view is in the positive *y* direction, and macroscopic variables are presented in normalized units.

magnetosheath separately and check for differences in FTE signatures. We select a region along a plane *xz* cutting the simulation volume at $y = 10$ (see Figure 5), for $t = 378$ s. This plane is approximately parallel to the direction of motion of the reconnected field lines and intersects the two regions of reconnected field lines formed above and below the diffusion region, in the *z* direction, which we call flux transfer event 1 (FTE 1) and flux transfer event 2 (FTE 2), respectively. Figure 6 shows the components of the magnetic field (Figure 6a) and plasma velocity (Figure 6b) normal to the nominal magnetopause (*x* component). Figure 6a shows that both FTEs produce bipolar signatures in the normal component of the magnetic field. This bipolar signature is due to the motion of plasma around the FTE, which bends the ambient magnetic field lines, and due to the twist of the magnetic field inside the FTE. If FTE 1 passes a satellite located in a position at $z > 0$, the satellite will observe a positive-negative pulse in the normal component of the magnetic field. This signature would correspond to a standard FTE in satellite data. If FTE 2 passes a satellite located in a position at $z < 0$, the satellite will see a negative-positive pulse in the normal component of the magnetic field. This signature would correspond to a reverse FTE in satellite data. Figure 6b shows that the FTEs are also associated with bipolar variations in the component of the velocity normal to the nominal magnetopause. The velocity variations are anticorrelated to magnetic field variations and are caused by the plasma motion around the FTE. There is no normal component of the velocity associated with the FTE itself. Figure 6 also reveals that there is an asymmetry between the signatures of FTE 1, which bulges into the magnetosphere, and FTE 2, which bulges into the magnetosheath, in the *x* components of velocity and magnetic field. This asymmetry is visible also in other plasma parameters. Figure 7 shows the plasma density (Figure 7a) and magnetic field intensity (Figure 7b). The density in FTE 1 increases compared with the density in the ambient magnetosphere. This increase in density is associated with a decrease in the total magnetic field and an increase in temperature (not shown here). The density in FTE 2 decreases compared with the ambient magnetosheath density. This density decrease is associated with an increase in the total field and an increase in temperature (not shown here). The total field decreases in the trailing edge of FTE 2, which is probably associated with the removal of magnetic flux from the reconnection region. The signature in plasma density and magnetic field related to FTE 2 presents a kind of vortical structure, which is not visible around FTE 1. From the results obtained here we conclude that the same FTE can have different signatures in satellite data, depending on whether the satellite encounters the part bulging into the magnetosphere or into the magnetosheath. A plane *xz* cutting the simulation volume at $y = -10$ would show a mirror image of what we have described in Figures 6 and 7, with FTE 1 now penetrating the magnetosheath and FTE 2 the magnetosphere. However, in this case, the bipolar variations in the velocity component normal to the nominal magnetopause would be correlated to the magnetic field variations. Again, this velocity is caused by plasma motion around the FTE tube, and the normal component of the magnetic field is an effect of the bending of magnetic field lines around it.

The distinct signatures from different trajectories relative to FTE 2 in the plane $y = 10L_0$ are presented in Figures 9–12. Figure 8 shows the four distinct trajectories T1, T2, T3, and T4. These trajectories have a length

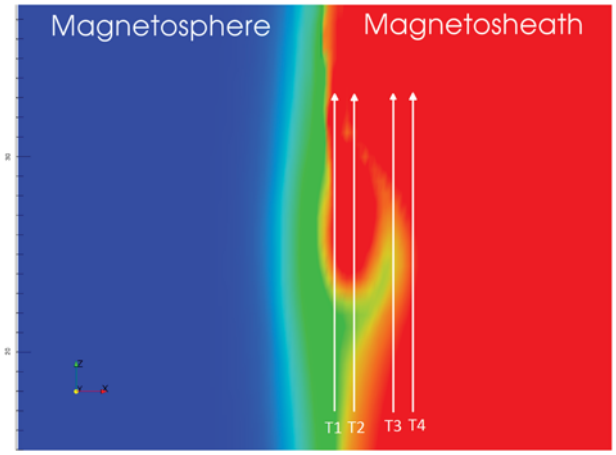

Figure 8. Plasma density near the magnetopause and four trajectories T1, T2, T3, and T4 in the plane $y = 10$ perpendicular to the magnetopause. The perturbed magnetopause region corresponds to the presence of a FTE located on the magnetosheath side of the magnetopause.

of $16L_0$ ($\approx$ 6400 km) along the z direction, parallel to the magnetopause, going from $z = 17L_0$ to $z = 33L_0$. Trajectory T1 is located at $x = 1L_0$, at 400 km from the center of the magnetopause into the magnetosheath. Trajectories T2, T3, and T4 are located at $x = 2L_0$ ($\approx$ 800 km), $x = 4L_0$ ($\approx$ 1600 km), and $x = 5L_0$ ($\approx$ 2000 km), respectively. Figure 9 shows the variations along trajectory T4 of the component of the magnetic field normal to the magnetopause (Figure 9, top, left), the total field strength (Figure 9, top, right), and density (Figure 9, bottom), in normalized units. The component of the magnetic field normal to the magnetopause presents the typical bipolar signature characteristic of FTEs. Trajectory T4 starts at the magnetosheath and skims the FTE. When approaching the transition region between the magnetopause and magnetosheath, the total field increases, and the plasma density decreases. At the center of the FTE the total field strength reaches its maximum, and the plasma density reaches its minimum, returning to magnetosheath values at the end of the trajectory. Figure10 shows the same signatures for trajectory T3. This trajectory starts in the magnetosheath and crosses the transition region. When crossing the transition region, the total field

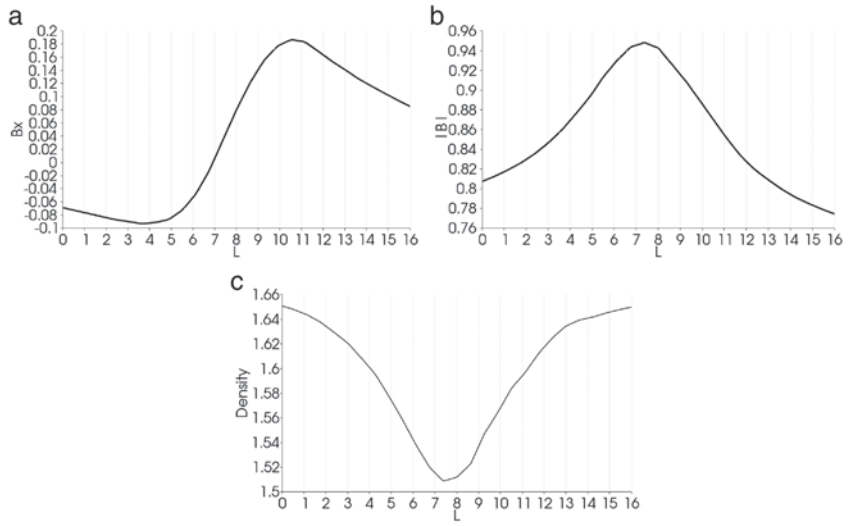

Figure 9. Plots of the component of the magnetic field normal to (top, left) the magnetopause, (top, right) the total field strength, and (bottom) plasma density for trajectory T4. This trajectory have a length of $16L_0$ ($\approx$ 6400 km) along the z direction, parallel to the magnetopause, going from $z = 17L_0$ to $z = 33L_0$, and is located at $x = 5L_0$ ($\approx$ 2000 km) from the center of the magnetopause into the magnetosheath. The x axis corresponds to the length of the trajectory starting from $z = 17L_0$. All plots are presented in normalized units.

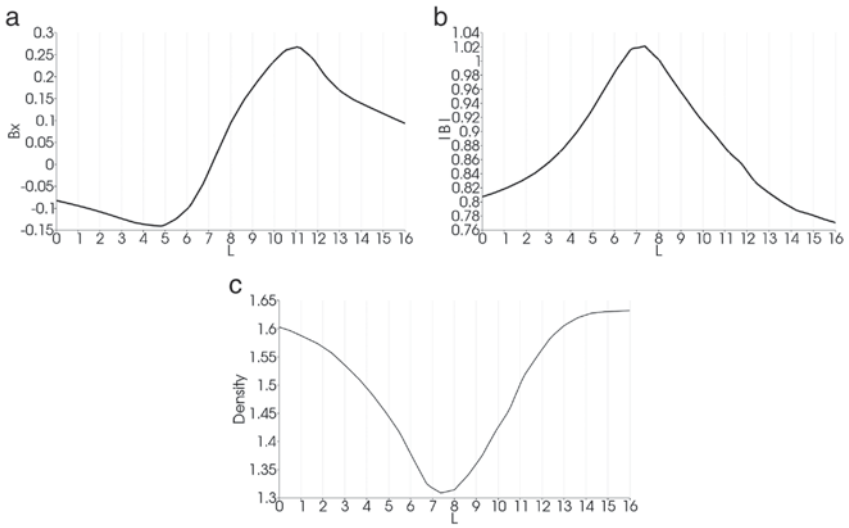

Figure 10. The same as Figure 9 but for trajectory T3 located at $x = 4L_0$ ($\approx$ 1600 km) from the center of the magnetopause into the magnetosheath.

strength (top, right) increases and the density (bottom) decreases, the peak values being larger than those obtained for trajectory T4. The results for trajectory T2 are presented in Figure11. This trajectory starts at the magnetosheath and crosses the FTE itself. The total field strength (top, right) increases and reach its maximum at the center of the FTE, where the component of the magnetic field normal to the magnetopause changes sign. At the trail part of the FTE the total field strength decreases to magnetosheath values. (bottom) The density decreases at the front part of the FTE, associated to the crossing of the magnetopause, and returns to increase inside the FTE itself reaching magnetosheath values. At the end of the trajectory the density decreases again since it crosses the transition region. The total field strength and the component of the magnetic field normal to the magnetopause start to increase at the end of the trajectory when entering the transition region. Figure 12 shows the signatures for trajectory T1. This trajectory starts at the magnetopause region and crosses the distorted magnetopause and transition region, returning to the magnetosheath at the end. The total field strength reaches its maximum at the center of the FTE and decreases below magnetosheath values at the end of the trajectory. Plasma density monotonically increases when crossing the FTE and at the end of the trajectory, when entering the magnetosheath. It is important to notice that the trajectories are not perpendicular to the axis of the FTE.

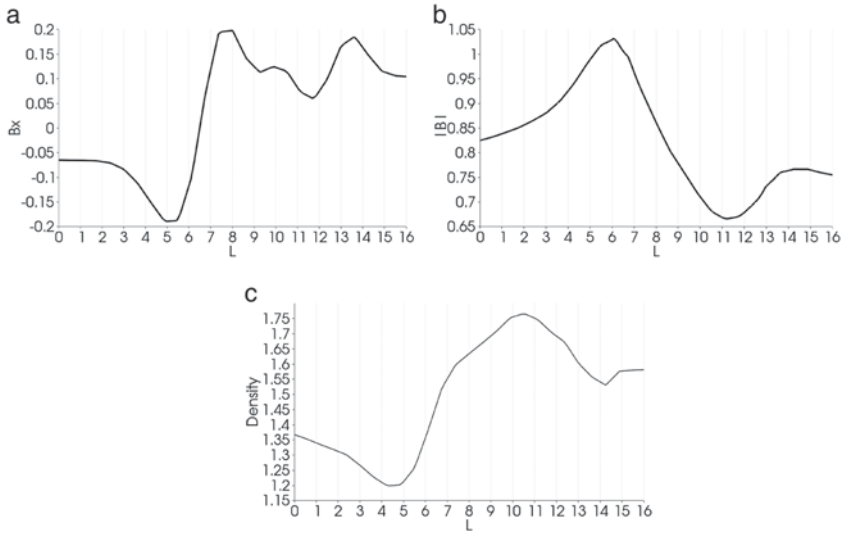

Figure 11. The same as Figure 9 but for trajectory T2 located at $x = 2L_0$ ($\approx$ 800 km) from the center of the magnetopause into the magnetosheath.

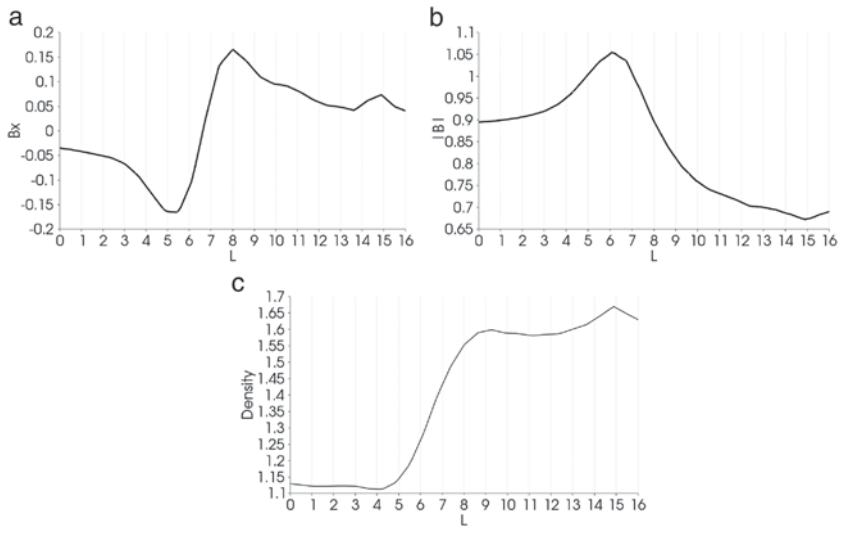

Figure 12. The same as Figure 9 but for trajectory T1 located at $x = 1L_0$ ($\approx$ 400 km) from the center of the magnetopause into the magnetosheath.

4. Summary and Conclusions

Our results show that a localized Petschek-type reconnection generates two regions of reconnected field lines above and below the diffusion region in the *z* direction, which we have called flux transfer event 1 (FTE 1) and flux transfer event 2 (FTE 2), respectively. At their initial stage the FTEs can be characterized as flux tubes since the newly reconnected magnetic field lines that form the FTE are not twisted. The FTEs move along the magnetopause plane, away from the reconnection site. During its motion the FTE displace the ambient plasma producing a bipolar signature in the component of the velocity normal to the nominal magnetopause. The plasma motion bends the ambient magnetic field producing a bipolar signature also in the component of the magnetic field normal to the nominal magnetopause. The bipolar magnetic field perturbation is also present in the core of the FTE while there is no bipolar velocity signature visible there. This indicates that during its evolution the magnetic field lines that form the FTE are twisted, and the FTE evolves from a flux tube to a flux rope configuration. The magnetic field twist is associated with electric currents along the FTE. Strong plasma jets are observed in the core of the FTE, and the combination of the bipolar flow field around the FTE and the jets gives a vortical flow pattern around the FTE.

Different from 2-D simulations or 3-D simulations where the magnetosheath and magnetospheric magnetic fields are perfectly antiparallel, here the FTE signature is not anymore associated with the bulge that forms around the field reversal region but it is distributed along the reconnected field lines as the Alfvenic perturbation propagates from the reconnection point. As a consequence, we are able follow the evolution of the part of the FTE bulging into the magnetosphere and the part bulging into the magnetosheath separately and check for differences in FTE signature. We identify significant differences between the signature of the FTE associated with the part that bulges into the magnetosphere and the part that bulges into the magnetosheath. In the part that bulges into the magnetosphere, the density increases inside the FTE compared to the ambient plasma. This density increase is associated with an increase in temperature, similar to the result obtained in the global simulations of *Raeder* [2006] and *Dorelli and Bhattacharjee* [2009]. The total magnetic field decreases inside the core of the FTE, characterizing a crater FTE. In the part that bulges into the magnetosheath, the density decreases inside the FTE compared to the ambient plasma. This density decrease is associated with an increase in temperature, as usually observed in FTEs. The total magnetic field also increases inside the FTE.

Acknowledgments

This work was supported by the DPP/UnB and CNPq under the project 482351/2012-8. Work at NASA/GSFC was supported by the THEMIS Explorer Mission.

Masaki Fujimoto thanks the reviewers for their assistance in evaluating this paper.

References

Büchner, J., and N. Elkina (2005), Vlasov code simulation of anomalous resistivity, *Space Sci. Rev.*, *121*, 237–252.

Büchner, J., and N. Elkina (2006), Anomalous resistivity of current-driven isothermal plasmas due to phase space structuring, *Phys. Plasmas*, *13*, 082304.

Cooling, B. M. A., C. J. Owen, and S. J. Schwartz (2001), Role of the magnetosheath flow in determining the motion of open flux tubes, *J. Geophys. Res.*, *106*, 18,763–18,775.

Cowley, S. W. H. (1984), Solar wind control of magnetospheric convection, in *Achievements of the International Magnetospheric Study (IMS),* Spec. Publ., ESA SP-217, pp. 483–494 pp, Eur. Space Agency, Noordwijk, Netherlands.

Dailey, R., C. A. Cattell, F. S. Mozer, and J. Berchem (1985), Electric fields and convection velocities associated with flux transfer events, *Geophys. Res. Lett.*, *12*, 843–846.

Dorelli, J. C., and A. Bhattacharjee (2009), On the generation and topology of flux transfer events, *J. Geophys. Res.*, *114*, A06213, doi:10.1029/2008JA013410.

Farrugia, C. J., R. C. Elphic, D. J. Southwood, and S. W. H. Cowley (1987), Field and flow perturbations outside the reconnected field line region in flux transfer events: Theory, *Planet. Space Sci.*, *35*, 227–240.

Fedder, J. A., S. P. Slinker, J. G. Lyon, and C. T. Russell (2002), Flux transfer events in global numerical simulations of the magnetosphere, *J. Geophys. Res.*, *107*(A5), 1048, doi:10.1029/2001JA000025.

Korotova, G. I., D. G. Sibeck, and T. Rosenberg (2009), Geotail observations of FTE velocities, *Ann. Geophys.*, *27*, 83–92.

Ku, H. C., and D. G. Sibeck (1997), Internal structure of flux transfer events produced by the onset of merging at a single X line, *J. Geophys. Res.*, *102*, 2243–2260.

Ku, H. C., and D. G. Sibeck (1998a), The effect of magnetosheath plasma flow on flux transfer events produced by the onset of merging at a single X line, *J. Geophys. Res.*, *103*, 6693–6702.

Ku, H. C., and D. G. Sibeck (1998b), Flux transfer events produced by bursty merging at a single X line, *J. Geophys. Res.*, *103*, 14,965–14,978.

Ku, H. C., and D. G. Sibeck (2000), Flux transfer events produced by the onset of merging at multiple X lines, *J. Geophys. Res.*, *105*, 2657–2675.

LaBelle, J., R. A. Treumann, G. Haerendel, O. H. Bauer, G. Paschmann, W. Baumjohann, H. Lühr, R. R. Anderson, H. C. Koons, and R. H. Holzworth (1987), AMPTE IRM observations of waves associated with flux transfer events in the magnetosphere, *J. Geophys. Res.*, *92*, 5827–5843.

La Belle-Hamer, A. L., A. Otto, and L. C. Lee (1995), Magnetic reconnection in the presence of sheared flow and density asymmetry: Applications to the Earth's magnetopause, *J. Geophys. Res.*, *100*, 11,875–11,889.

Liu, J., V. Angelopoulos, D. Sibeck, T. Phan, Z. Y. Pu, J. McFadden, K. H. Glassmeier, and H. U. Auster (2008), THEMIS observations of the dayside traveling compression region and flows surrounding flux transfer events, *Geophys. Res. Lett.*, *35*, L17S07, doi:10.1029/2008GL033673.

Ma, Z. W., L. C. Lee, and A. Otto (1995), Generation of field-aligned currents and Alfvén waves by 3D magnetic reconnection, *Geophys. Res. Lett.*, *22*, 1737–1740.

Otto, A. (1990), 3D resistive MHD computations of magnetospheric physics, *Comput. Phys. Commun.*, *59*, 185–195.

Otto, A. (1995), Forced three-dimensional magnetic reconnection due to linkage of magnetic flux tubes, *J. Geophys. Res.*, *100*, 11,863–11,874.

Otto, A., L. C. Lee, and Z. W. Ma (1995), Magnetic field and plasma properties associated with pressure pulses and magnetic reconnection at the dayside magnetopause, *J. Geophys. Res.*, *100*, 14,895–14,911.

Paschmann, G., G. Haerendel, I. Papamastorakis, N. Sckopke, S. J. Bame, J. T. Gosling, and C. T. Russell (1982), Plasma and magnetic field characteristics of magnetic flux transfer events, *J. Geophys. Res.*, *87*, 2159–2168.

Petschek, H. E. (1964), The physics of solar flares, in *Proceedings of the AAS-NASA Symposium held 28-30 October, 1963 at the Goddard Space Flight Center*, edited by W. N. Hess, pp. p. 425, Natl. Aeronaut. Space Administration, Sci., and Tech. Inf. Div., Washington, D. C.

Raeder, J. (2006), Flux transfer events: 1. Generation mechanism for strong southward IMF, *Ann. Geophys.*, *24*, 381–392.

Rijnbeek, R. P., S. W. H. Cowley, D. J. Southwood, and C. T. Russell (1984), A survey of dayside flux transfer events observed by ISEE 1 and 2 magnetometers, *J. Geophys. Res.*, *89*, 786–800.

Russell, C. T., and R. C. Elphic (1978), Initial ISEE magnetometer results—Magnetopause observations, *Space Sci. Rev.*, *22*, 681–715.

Santos, J. C., and J. Büchner (2007), MHD simulation of electric currents in the solar atmosphere caused by photospheric plasma motion, *Astrophys. Space Sci. Trans.*, *3*, 29–33.

Santos, J. C., J. Büchner, M. S. Madjarska, and M. V. Alves (2008), On the relation between DC current locations and an EUV bright point: A case study, *Astron. Astrophys.*, *490*, 345–352.

Santos, J. C., J. Büchner, and A. Otto (2011a), Development of electric currents in a magnetic field configuration containing a magnetic null point, *Astron. Astrophys.*, *525*(A3), 13.

Santos, J. C., J. Büchner, and A. Otto (2011b), 3D MHD simulations of electric current development in a rotating sunspot: Active region NOAA 8210, *Astron. Astrophys.*, *535*(A111), 9.

Saunders, M. A., C. T. Russell, and N. Sckopke (1984), Flux transfer events: Scale size and interior structure, *Geophys. Res. Lett.*, *11*, 131–134.

Tóth, G. (2000), The $\nabla \cdot B = 0$ constraint in shock-capturing magnetohydrodynamics codes, *J. Comput. Phys.*, *161*, 605–652.

Zhang, H., K. K. Khurana, M. G. Kivelson, V. Angelopoulos, Z. Y. Pu, Q.-G. Zong, J. Liu, and X.-Z. Zhou (2008), Modeling a force-free flux transfer event probed by multiple Time History of Events and Macroscale Interactions during Substorms (THEMIS) spacecraft, *J. Geophys. Res.*, *113*, A00C05, doi:10.1029/2008JA013451.

Zhang, H., et al. (2010), Evidence that crater flux transfer events are initial stages of typical flux transfer events, *J. Geophys. Res.*, *115*, A08229, doi:10.1029/2009JA015013.

Zhang, H., M. G. Kivelson, V. Angelopoulos, K. K. Khurana, R. J. Walker, Y. D. Jia, J. McFadden, and H. U. Auster (2011), Flow vortices associated with flux transfer events moving along the magnetopause: Observations and an MHD simulation, *J. Geophys. Res.*, *116*, A08202, doi:10.1029/2011JA016500.